# Infrared Limb Sounding — MIPAS and HIRDLS

**Anu Dudhia**

*Atmospheric, Oceanic and Planetary Physics*
*Oxford University, Oxford, UK*

## 1 Introduction

Limb-sounding has several advantages over nadir-sounding for the retrieval of atmospheric temperature and composition: improved vertical resolution, the ability to retrieve at higher altitudes and increased sensitivity to minor species through the airmass weighting and contrast against the cold background of space.

The disadvantages are poorer horizontal resolution and, for infrared instruments, less tropospheric coverage due to the increased likelihood of cloud contamination. However, the presence of cloud need not affect the quality of the retrieved profile at higher levels.

The limb-viewing geometry also introduces additional complications in the forward modelling and retrieval procedure. These are illustrated using examples of two instruments representing extremes of spectral and spatial resolution.

## 2 Limb Sounding

### 2.1 Geometry

Nadir-sounding can be regarded as a one-dimensional (vertical) problem, but limb-sounding in or near the orbit plane is two-dimensional since the ray-paths traverse a significant horizontal distance through the atmosphere. Although retrieved profiles are often assigned a single geographic location (i.e., 'vertical') Figs.1 and 2 show that the location of the tangent points which contribute to each profile level can be displaced by of the order of 100 km from top to bottom of the profile. Even if the vertical scan is timed so that the tangent points lie along a vertical line the region of the atmosphere which contributes most may lie somewhere between the tangent point and the satellite.

### 2.2 Instruments

Table 1 lists various infrared limb sounders flown to date or to be launched in the near future. These can be classified into two types: radiometers and spectrometers.

Radiometers have predefined spectral channels, usually of widths of the order of 10s of $cm^{-1}$ (or a few % of the wavelength) and each designed to capture emission features from a particular molecule. Such instruments are relatively simple in principle, and have the advantage of good signal/noise which can be traded off against spatial resolution.

Spectrometers measure the complete spectrum within particular limits at high resolution, but only subsets of these spectra are required for the retrieval of particular species. Three different types of spectrometer have been used: Fourier transform (MIPAS, TES), grating (CRISTA) and etalon (CLAES). Signal/noise is usually a limiting factor since only a finite number of photons are received in each spectral channel, and this tends to

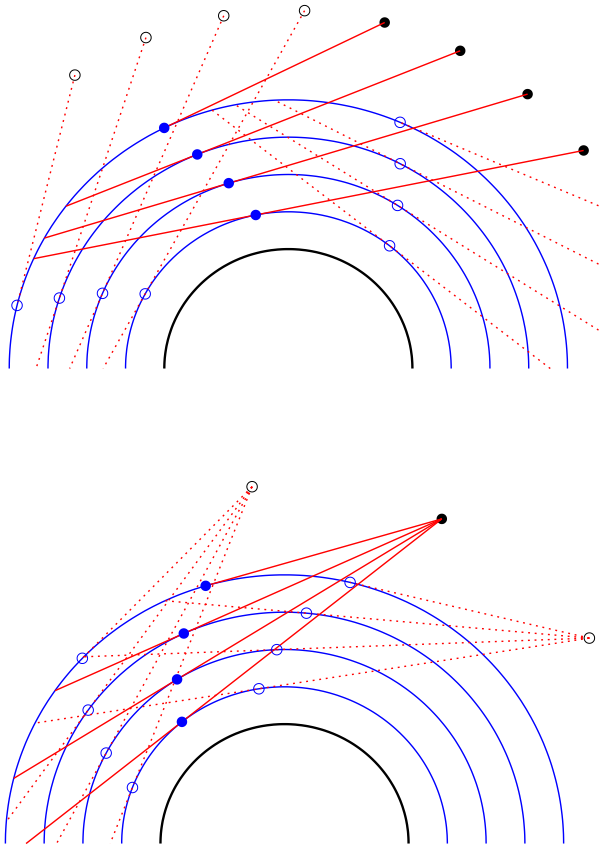

*Figure 1: Two examples of limb sounding measurements (exaggerated scale). In both cases the satellite is moving clockwise and viewing rearward in the orbital plane. The top diagram shows the case for a slow, downward limb scan, e.g. MIPAS. Here the locus of tangent points largely follows the satellite motion and slopes away from the satellite with increasing altitude. The bottom diagram represents an instrument with a fixed detector array or a fast vertical scan, e.g. HIRDLS. Here the satellite motion is negligible during the time taken to acquire the measurements for a single profile and the locus of the tangent points slopes towards the satellite with increasing altitude.*

*Table 1: Infrared limb sounding instruments.*

| Launch | Satellite | Instrument(s) |
|---|---|---|
| 1976 | Nimbus 6 | LRIR$^r$ |
| 1978 | Nimbus 7 | LIMS$^r$, SAMS$^r$ |
| 1991 | UARS | CLAES$^s$, ISAMS$^r$ |
| 1994, 1997 | Shuttle | CRISTA$^s$ |
| 2001 | Envisat | MIPAS$^s$ |
| 2001 | TIMED | SABER$^r$ |
| 2004? | Aura | HIRDLS$^r$, TES$^s$ |

$^r$Radiometer, $^s$Spectrometer

favour the Fourier transform instruments despite their mechanical complexity (grating spectrometers are more commonly used for solar occultation).

In this article, one spectrometer (MIPAS) and one radiometer (HIRDLS) will be considered in detail.

### 2.3 MIPAS

The Michelson Interferometer for Passive Atmospheric Sounding (ESA, 2000) was launched on ESA's Envisat satellite on 1st March 2002. MIPAS is a Fourier transform spectrometer with a maximum optical path difference of 20 cm, giving spectra sampled at 0.025 $cm^{-1}$ (actual resolution is closer to 0.035 $cm^{-1}$), split into 5 bands in the range 685–2410 $cm^{-1}$ (14.5–4.1 $\mu$m), MIPAS views the atmospheric limb with a field-of-view approximately 3 km $\times$ 30 km (height$\times$width). Usually viewing is in the rearward direction although it also has the capability to view sideways. In the nominal observing mode, a spectrum is acquired every 4.6 seconds at each of 17 tangent altitudes starting at 68 km and finishing at 6 km (3 km steps between 42–6 km). A complete limb scan is obtained approximately every 80 seconds, or 500 km along-track (Fig.2), giving over 1000 profiles a day.

### 2.4 HIRDLS

The High Resolution Dynamics Limb Sounder (Gille *et al.*, 1994) is due to be launched on NASA's Aura satellite early in 2004. HIRDLS is a 21-channel infrared limb scanning radiometer, each channel having an instantaneous FOV of 1 km $\times$ 10 km (height$\times$width). The instrument looks to the rear of the satellite and scans continuously rather than in discrete steps, taking approximately 3.75 s to scan the tangent height range 5–80 km. The current plan is to take 7 limb scans at 6 different azimuth angles, with one track sampled twice, in a complete cycle lasting 67 s (including calibration black-body and space views). This gives approximately 9000 profile locations per day, spaced at 500 km along 5 azimuth tracks and 250 km for the double-sampled track.

## 3 Channel Selection

### 3.1 The Infrared Spectrum

The infrared region of the atmospheric emission spectrum is characterised by the vibration-rotation transitions of many different molecules. For remote-sensing purposes the useful range lies within 500–2500 $cm^{-1}$ (4–20$\mu$m), the long wavelength limit being set by increasing $H_2O$ absorption (and detector technology) while the shorter wavelengths are affected by the increasing contribution of scattered solar radiation and other non-LTE processes which are difficult to model.

Figs. 3 and 4 show the spectral features of the principal emitting species and the locations of HIRDLS channels and MIPAS microwindows.

### 3.2 Radiometer Channels

Radiometer channels are selected to maximise the contribution of a particular molecule while minimising those of other species (Edwards *et al.*, 1995). Narrow channels give better spectral discrimination but reduced signal/noise.

Fig. 5 shows the temperature Jacobians (or weighting functions) for different tangent altitudes for the four HIRDLS channels located across the 667 $cm^{-1}$ (15$\mu$m) $CO_2$ band. Channel 5, situated in the strongest part of the band, has strongly peaked Jacobians at high altitude, indicating good vertical resolution, but these become broader below 30 km as the opacity in this part of the spectrum increases (actually more similar to nadir-sounding Jacobians). HIRDLS uses four channels situated in different parts of the $CO_2$ band to ensure optimal

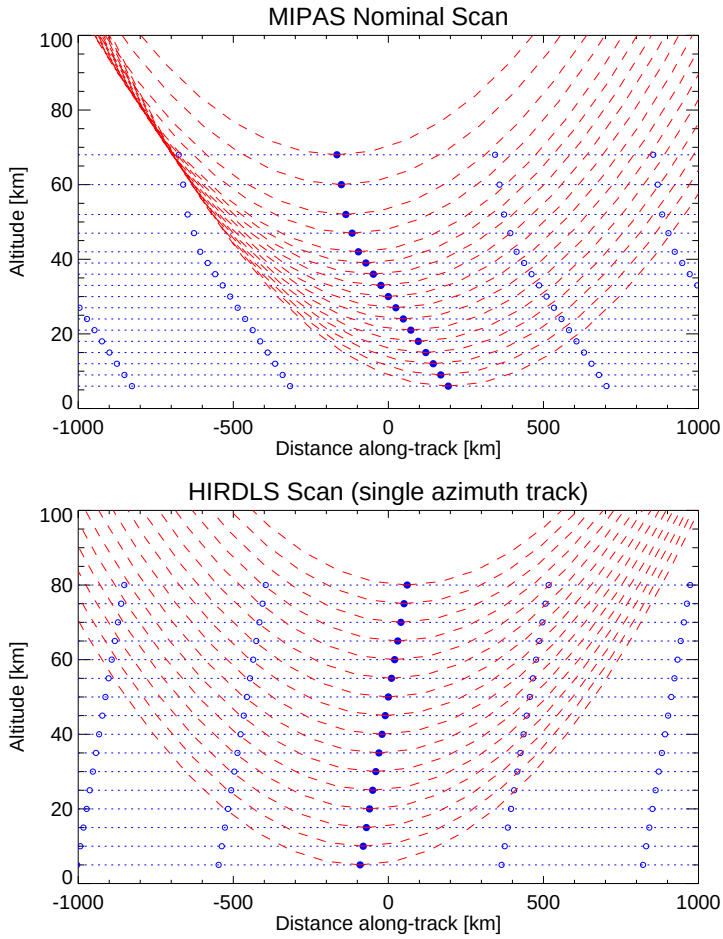


*Figure 2: The tangent paths (dashed) and tangent points (solid circles) for nominal MIPAS (top) and HIRDLS (bottom) rear-viewing limb scans, with the satellite to the right and moving right in both cases. Open circles show tangent points from successive scans. The HIRDLS plot represents just one of the five single-sampled azimuth tracks, a sixth track is sampled at twice this rate.*

temperature retrievals over the complete altitude range. Similarly there are three $O_3$ channels and two $H_2O$ channels.

### 3.3 Microwindow Selection

Microwindows are defined as 'rectangular' subsets of the measurement domain, defined by upper and lower boundaries in both wavenumber and tangent altitude axes. However, this differs from a radiometer filter in that each spectral point is kept distinct and assigned a weight appropriate to its Jacobian (i.e., signal) and noise contributions.

There are computational advantages in modelling radiances from adjacent points in this domain, as opposed to using isolated measurements, but the main advantage is that a spectrally flat atmospheric continuum can be retrieved for each microwindow (Clarmann and Echle, 1998). In effect, the signal used for the retrieval of the target species is measured from the line peaks relative to this continuum baseline rather than in absolute radiance. This is useful for eliminating the effects of thin cloud or aerosols, or far wings of strong lines of other species, but does make the retrieval of heavy molecules (which lack distinct line spectra) more difficult.

A characteristic of the MIPAS microwindows is the use of spectral masks, i.e., not all points within the microwindow are used in the retrieval. This allows measurements which might introduce large systematic errors,

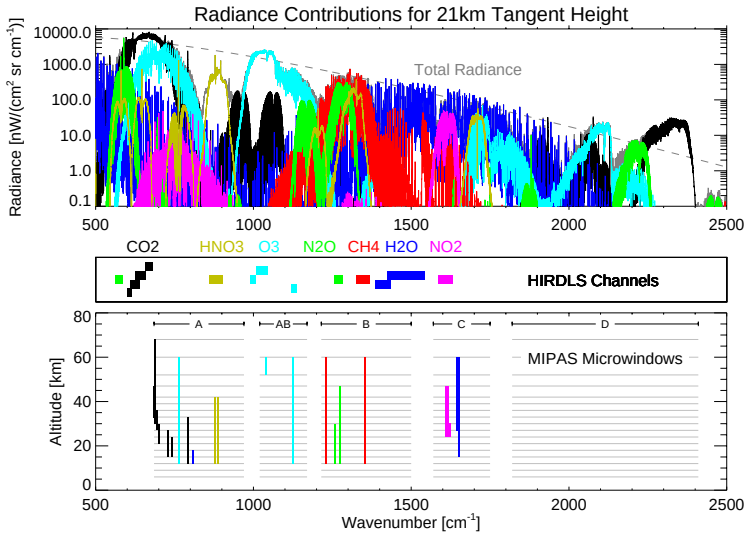


*Figure 3: Simulated infrared limb emission spectrum showing the contributions of the major species, together with the current MIPAS microwindows and HIRDLS channels. The grey spectrum is the total radiance for all absorbers (more visible in Fig. 4) and the dashed line is the Planck function for the tangent point temperature (218 K).*

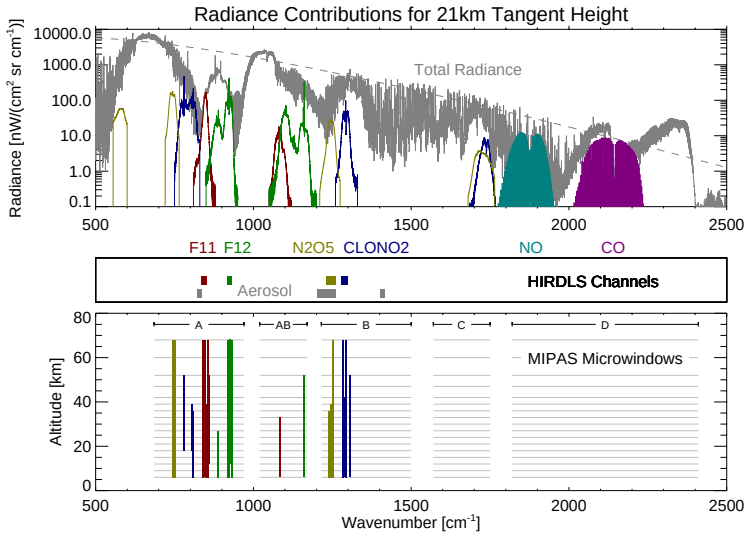


*Figure 4: As Fig. 3 except showing additional species and proposed MIPAS microwindows. The CO and NO emissions are strongly affected by non-LTE and their retrieval is not anticipated to form part of ESA's operational processing.*

e.g., because they coincide with lines from an interfering species, to be assigned zero weight irrespective of their Jacobian weight.

The MIPAS microwindows and masks have been selected using a computer algorithm which attempts to minimise the total of the random and systematic error components in the retrieved profile (Echle *et al.*, 2000, Dudhia *et al.*, 2002). One aspect of this computational selection is that masks are often placed in non-intuitive

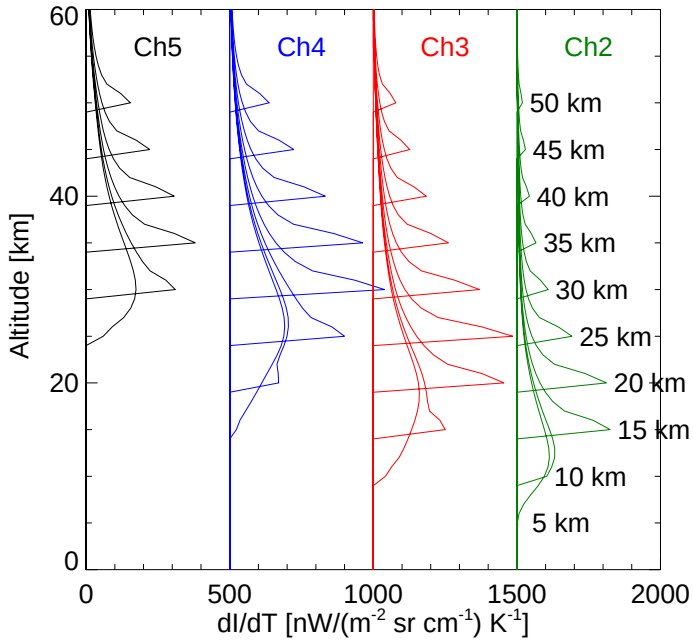


*Figure 5: Temperature Jacobians for HIRDLS Channels 2 (600.5–614.75 cm$^{-1}$) 3 (610–639.5 cm$^{-1}$), 4 (626–660 cm$^{-1}$) and 5 (655–680 cm$^{-1}$) for tangent heights at 5 km intervals. Channels are offset horizontally for clarity. The y-axis indicates altitude of the temperature perturbation while the figures on the right indicate measurement tangent height, plotted at 5km intervals.*

positions, either to cancel out systematic errors or to divert them into the continuum retrieval.

Fig. 6 shows an example of a MIPAS microwindow for a $pT$ retrieval. Note that masks have been placed over the opaque centre of the strong emission line at 728.6 cm$^{-1}$ to reduce horizontal gradient effects, and also over the strong water vapour line at the high wavenumber boundary.

### 3.4 Data Products

Table 2 lists some of the parameters retrievable with MIPAS and HIRDLS.

## 4 Radiance Modelling

### 4.1 Radiative Transfer

The spectral radiance from an infinitesimal solid angle represents an integration of the radiative transfer equation through the atmosphere

$$L = \int B(s) \frac{d\tau(s)}{ds} ds \tag{1}$$

where $B$ is the Planck function for the local temperature along the path coordinate $s$ and $\tau$ is the transmittance from $s$ to the satellite (assuming a non-scattering atmosphere in local thermodynamic equilibrium).

Fig. 7 shows how this is calculated numerically. The atmosphere is divided into a series of shells (of which the retrieval levels usually form a subset) and the ray path in each shell approximated by an equivalent homoge-

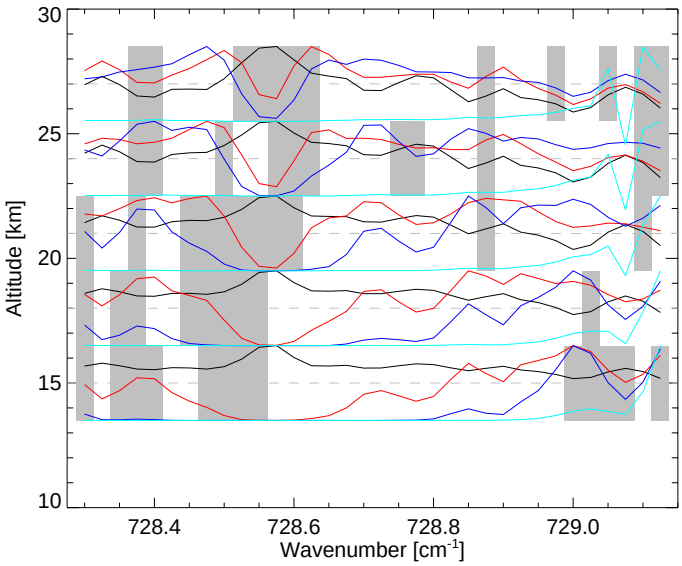


*Figure 6: The MIPAS PT_0004 microwindow, used for retrieving temperature and pressure between 15–27 km. Grey areas indicated measurements which are masked out, the black lines at each tangent altitude are the measured spectra, the red lines are the Jacobian spectra for temperature perturbations at the tangent point, blue lines for pressure Jacobians and turquoise lines for the interference signal from water vapour (all spectra scaled to same amplitude).*

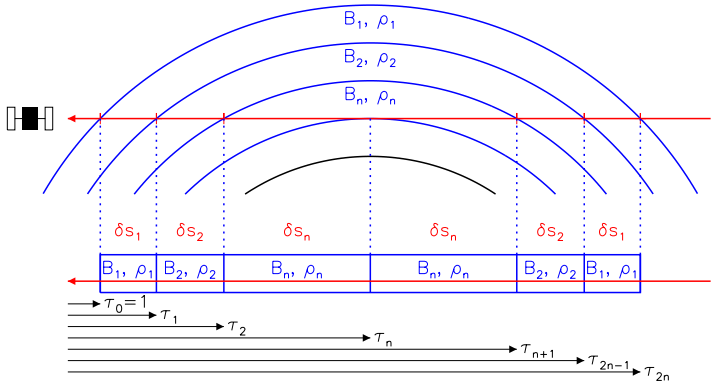


*Figure 7: Radiative transfer for limb paths. The inhomogeneous atmospheric path is replaced by an equivalent path through a series of homogeneous cells.*

neous path containing the same absorber mass $\int \rho \, ds$ at the absorber-weighted mean temperature and pressure ('Curtis-Godson' approximation)

$$L \simeq \sum_i B_i \delta\tau_i \tag{2}$$

where $\delta\tau_i$ represents the change in transmittance across cell $i$ (Fig. 7).

For 'monochromatic' calculations (i.e., at a discrete wavenumber $\nu$) the transmittance $\tau_i$ to any boundary $i$ is simply the product of the transmittances of all component cells $\tau_j^c$ (Beer's Law), so that

$$\delta\tau_i \quad = \quad \tau_{i-1} - \tau_i \tag{3}$$

*Table 2: Atmospheric parameters retrieved from MIPAS and HIRDLS together with the altitude ranges. For MIPAS the table shows the standard ESA products and current altitude ranges, together with possible future extensions. For HIRDLS these are the predicted ranges. Lower altitudes assume cloud-free scenes.*

| Species | MIPAS | | HIRDLS |
|---|---|---|---|
| | Current | Future | Estimated |
| $pT$ | 12–68 km | 6–68 km | 7–80 km |
| $H_2O$ | 12–60 km | 6–68 km | 7–70 km |
| $O_3$ | 12–60 km | 6–68 km | 10–80 km |
| $HNO_3$ | 12–42 km | 9–42 km | 10–40 km |
| $CH_4$ | 12–60 km | 6–68 km | 10–65 km |
| $N_2O$ | 12–47 km | 6–60 km | 10–55 km |
| $NO_2$ | 24–47 km | 24–68 km | 20–60 km |
| Aerosol[a] | 12–30 km | 6–30 km | 10–30 km |
| CFC-12 | - | 6–30 km | 7–30 km |
| $ClONO_2$ | - | 18–39 km | 17–40 km |
| $N_2O_5$ | - | 15–33 km | 20–45 km |
| CFC-11 | - | 6–21 km | 7–28 km |
| CFC-14 | - | 12–52 km | - |
| HCFC-22 | - | 6–24 km | - |
| $NH_3$ | - | 6–21 km | - |
| HCN | - | 12–18 km | - |
| $COF_2$ | - | 15–33 km | - |
| OCS | - | 9–24 km | - |
| $SF_6$ | - | 6–21 km | - |
| $C_2H_6$ | - | 6–15 km | - |
| HOCl | - | 18–30 km | - |
| $SO_2$ | - | 12–18 km | - |

[a]explicit product for various HIRDLS channels, but a by-product for each MIPAS microwindow

$$= \quad (1-\tau_i^c)\prod_{j=1}^{i-1}\tau_j^c \tag{4}$$

This breaks the radiative transfer down into two main parts: the ray tracing and the calculation of cell transmittances.

## 4.2 Ray Tracing

To calculate the path $s$ through the atmosphere it is usually adequate to assume that the earth is spherical, but a fairly simple improvement can be obtained if the local radius of curvature is used rather than a global average ($\pm 0.5\%$ variation around the orbit).

Refraction is a more significant effect, lowering the tangent point and increasing the path length through the atmosphere. The effect becomes significant at around 25 km altitude, at which level the tangent point is displaced by 70 m vertically, or about 1% in pressure, but increases in proportion to air density.

The Curtis-Godson equivalent parameters are calculated by numerical integration, conveniently performed in parallel with the ray-tracing.

### 4.3 Transmittance Calculation

The transmittance of a particular cell $\tau^c$ is derived from the sum of the contributions of each absorbing species $g$

$$\tau = \exp - \sum_g \int k_g \rho_g \, ds \tag{5}$$

The absorption coefficient $k$ of a molecule at wavenumber $\nu$ is the sum of all transitions centred at nearby wavenumbers $\nu_l$

$$k = \sum_l S_l \, f_l(\nu - \nu_l) \tag{6}$$

where $S_l$ is the line strength and $f_l$ is the lineshape factor for transition $l$. Line strength is a function of local temperature and lineshape a function of temperature, pressure, and, in the case of high concentrations, water vapour. This is the summation performed by 'line-by-line' models.

### 4.4 Measurement Simulation

The satellite measurement $R_{mt}$ in a particular channel $m$ from elevation angle (or tangent path) $t$ represents a convolution of the spectral radiance $L$ reaching the satellite with the instrument field-of-view $\Phi$ and channel spectral response $\Psi$ functions.

$$R_{mt} = \int \int L(\nu, \theta) \Phi(\theta - \theta_t) \Psi(\nu - \nu_m) \, \mathrm{d}\nu \mathrm{d}\theta \tag{7}$$

where $\nu$ is the wavenumber and $\theta$ is the elevation angle.

The radiance field $L$ varies relatively smoothly with tangent altitude so that the numerical convolution with the field-of-view is not a major overhead, especially if radiance calculations are performed for several different elevation angles simultaneously.

However, the spectral structure of atmospheric radiances varies on a fine scale, typically requiring calculations at 0.0005 $\mathrm{cm}^{-1}$ resolution to capture the emission features of Doppler-broadened line centres which, although narrow, contribute a significant amount of integrated radiance. Thus, even for high resolution spectrometers such as MIPAS, each 0.025 $\mathrm{cm}^{-1}$ 'measurement' requires radiance to be computed at 50 spectral points for an accurate simulation (Figs. 8).

### 4.5 MIPAS Forward Model

The line-by-line calculation (Eq. 6) often requires summation over many hundreds of lines in order to compute the absorption coefficient for a single wavenumber at a particular cell pressure and temperature $k(\nu, p^c, T^c)$.

The operational processing of MIPAS data (Ridolfi *et al.*, 2000) avoids this by using look-up tables of pre-computed values of $k(\nu, p, T)$ and simply interpolates in the pressure and temperature domains for the required values (Singular Value Decomposition is also used to compress these tables to a reasonable size (Dudhia *et al.*, 2002b).

A further advantage of using look-up tables is that the derivatives of $k$ with respect to pressure and temperature can simply calculated from the differences in table entries along the $p$ and $T$ axes.

A second optimisation is to only compute the radiative transfer at a subset of 0.0005 $\mathrm{cm}^{-1}$ grid points: using full resolution where the structure of the spectrum field is most detailed and lower resolution and linear interpolation in the flatter regions between lines. This is shown in Fig. 9.

Both these optimisations introduce some level of interpolation error compared with a line-by-line calculation on the full spectral grid. However, the error can be made arbitrarily small by adding further points and the

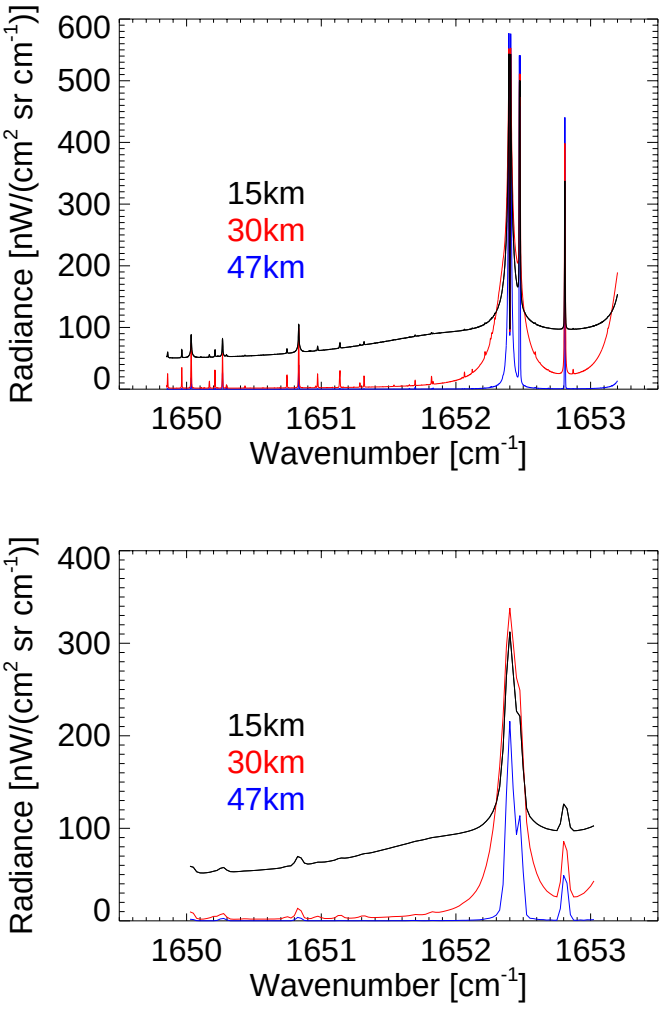


*Figure 8: Monochromatic spectra (top) calculated at 0.0005 $cm^{-1}$ resolution for three different tangent heights for the MIPAS H2O_0001 microwindow and simulated measurements (bottom) at 0.025 $cm^{-1}$ resolution after convolution with the apodised instrument lineshape.*

actual criterion chosen was that the total interpolation error should be no more than one tenth of the random noise, i.e., negligible. Nevertheless, compared to the full line-by-line calculation, a reduction in computing time of one or two orders of magnitude is obtained.

### 4.6 HIRDLS Forward Model

HIRDLS channels are much wider than MIPAS microwindows, and measurements are more frequent, so a radically different approach is used. This is to precompute the spectral convolution with channel response, so that for a particular channel Eq. 2 effectively becomes (Marks and Rodgers, 1993)

$$\bar{L}^m = \sum_i \bar{B}^m \delta\bar{\tau}_i^m \quad (8)$$

$$\delta\bar{\tau}_i^m = \bar{\tau}_{i-1}^m - \bar{\tau}_i^m \quad (9)$$

where for some parameter $x$ and channel $m$, $\bar{x}^m$ denotes $\int x(\nu)\Psi(\nu-\nu_m)d\nu$. In fact, HIRDLS radiances are 'deconvolved' in the vertical domain as part of the Level 1 processing, so Eq.7 is omitted completely since $\bar{L}^m$

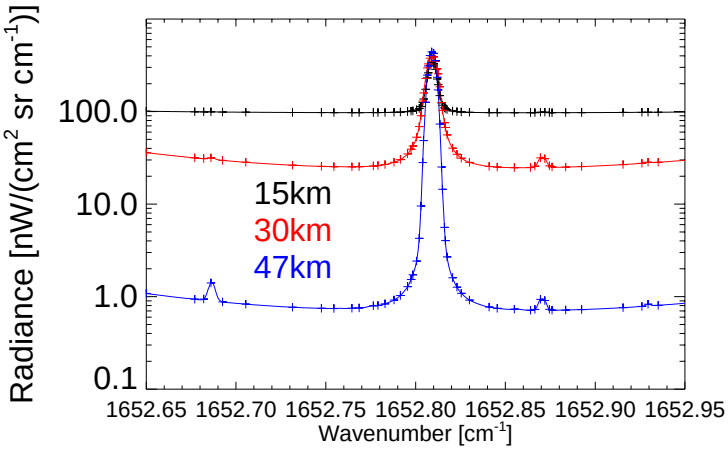


*Figure 9: Detail of Fig. 8, crosses marking the points where the monochromatic spectra are actually calculated in the MIPAS forward model.*

is the actual measurement.

The only integration now required is along the tangent path, this is significantly faster than even the MIPAS approach. However, there are limitations, in particular that Beer's Law does not hold for averaged transmittances so that Eq. 4 cannot be used to decompose the path transmittance into the product of cell transmittances.

Instead, the complete path transmittances $\overline{\tau}_i$ have to be pretabulated. In principle this requires a tabulation in terms of all atmospheric parameters from the satellite to boundary $i$, but in practice only three are used for each absorbing species: pressure, temperature and absorber amount. The atmospheric path transmittance for each species is then represented by a single equivalent homogeneous path containing the same absorber amount and using either the Curtis-Godson or the Emissivity Growth approximations (Weinreb and Neuendorffer, 1973) to obtain the equivalent pressure and temperature. Furthermore, it is assumed that the total path transmittance for all species is the product of the transmittance for each species (i.e., that the lines each species are randomly positioned with respect to each other — a better approximation with wide channels than with narrow channels).

This has the same advantages for computing Jacobians as the MIPAS 'monochromatic' look-up tables. However, unlike the monochromatic approach, it cannot be made 'asymptotically' accurate simply by adding more points to the tables, and there is probably a fundamental inaccuracy of the order of 0.5–1% using this method compared with a line-by-line model.

# 5 Retrievals

## 5.1 Retrieval Grids

In nadir sounding it is natural to retrieve on pressure levels since Jacobians are largely determined by pressure and vertical radiative transfer can be performed in pressure coordinates.

For the same reasons, altitude is the natural coordinate for limb sounding. However, the absolute altitude of the tangent point is generally not well-known since it involves an accurate knowledge of the satellite pitch angle: typical accuracy is $\pm 1$ arc minute, corresponding to $\sim \pm 1$ km when projected on to the limb 3000 km away. This is not as serious a problem as it may first seem since limb radiances are insensitive to absolute altitude,

apart from a small effect due to the increased path length. Nevertheless, in order to perform the ray-tracing and radiative transfer it is necessary to establish the temperature, pressure and location of the tangent points on some accurate *relative* altitude scale.

For a set of tangent points $t$, the alternatives are

1. Retrieve parameters at the tangent points themselves, $T(t), p(t)$
2. Retrieve parameters on an altitude scale $T(z'), p(z')$ with altitude $z'$ defined relative to some reference tangent point $t_{\mathrm{ref}}$
3. Retrieve parameters, including tangent point, on pressure levels $T(p), t(p)$.

Option 1 allows for some uncertainty in relative pointing knowledge ($\pm$150 m in the case of MIPAS) and uses the hydrostatic equation (Eq. 10) to establish relative altitudes.

Option 2 assumes relative tangent point altitudes are well-known, e.g., if the instrument uses a detector array with fixed elevation angles or, as in the case of HIRDLS, precise relative pointing information is obtainable from gyroscopes attached to the optical bench.

Option 3 is equivalent to either option 1 or 2, according to the quality of the relative pointing information. While this does not fully exploit the potential vertical resolution by retrieving on the tangent points, it is convenient if the retrieved profiles are to be used in conjunction with some model since it avoids an extra reinterpolation in profile space.

### 5.2 Hydrostatic Constraints

Whichever option is used, fundamentally only $p$ and $T$ are retrievable from the radiances but a third parameter, $z$, is also required for the forward model. The three are linked in the atmosphere via the hydrostatic equation:

$$d \ln p = -\frac{gM}{RT} dz \tag{10}$$

where $g$ is the acceleration due to gravity, $M$ is the molar air mass, $R$ is the molar gas constant. It should be noted that this is not strictly applicable to slanting profiles but the error induced by horizontal gradients is relatively small.

Retrieving $p$ and $T$ from a single tangent altitude requires at least two measurements with different sensitivities to pressure and temperature. At low altitudes radiometers can rely on the contrast between saturating/non-saturating channels, indicated by the intersecting contours in Fig. 10 — saturating channels start to become insensitive to pressure. At high altitudes, however, pressure sensitivity becomes linear in all cases and there is more ambiguity, indicated by the parallel contours.

This is less of a problem for spectrometers since individual lines can usually be found with strongly varying temperature sensitivities within each microwindow (note also the contrasting shapes of the pressure and temperature Jacobians in Fig. 6. However, at high altitudes the accuracy is still limited by low signal/noise.

In order to resolve this, it is usually necessary to include some relative pointing information $z$ from the instrument itself, either as a 'soft' *a priori* constraint (Option 1, as used for MIPAS) or, if well-known, as a 'hard' constraint (Option 2).

### 5.3 Retrieval Sequence

Temperature is a fundamental parameter in infrared emission, mostly through the Planck Function but also through air density (therefore absorber concentrations), and absorption coefficients (line strength and line

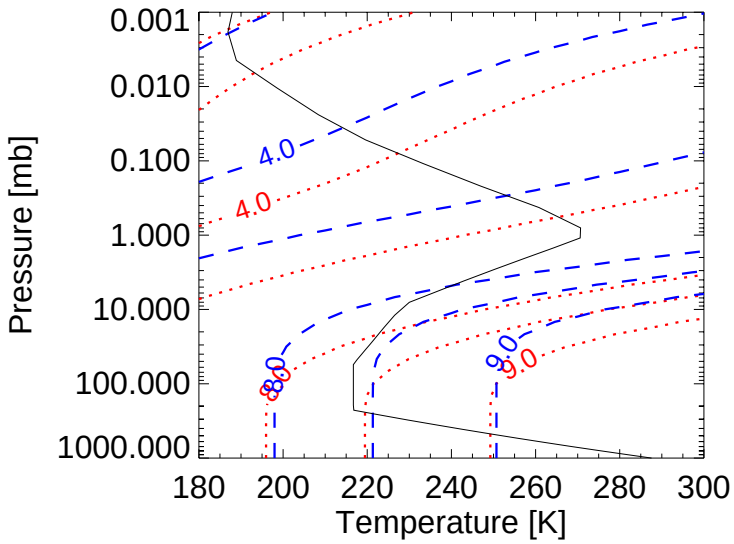


*Figure 10: Radiance contours for HIRDLS Channels 3 (red,dotted) and 4 (blue,dashed) as a function of tangent point pressure and temperature, with the US Standard Atmosphere $T(p)$ profile superimposed (black,solid) to indicate the expected regime. See also Fig. 5.*

shape). The sensitivity of the Planck function to temperature in the mid-infrared is approximately ∼4%/K which imposes an immediate requirement for temperature retrieval accuracy <2.5 K if composition is to be retrieved to better than 10%.

Radiance is less sensitive to pressure, proportional to $p$ in the optically thin limit, but proportional to $p^2$ where Lorentz broadening becomes significant. However, pressure is important in establishing the pointing/coordinate system for the limb-viewing geometry.

For these reasons infrared limb retrievals usually start with a joint retrieval of pressure and temperature using radiance measurements from a region of the spectrum where the emission is primarily from a gas of known volume mixing ratio, i.e., $CO_2$.

Having established temperature and pressure, other species can then be retrieved in a sequence determined by their contaminating effects in other channels. For example, water vapour has significant emission features throughout the entire infrared spectrum so is often retrieved early in the sequence and the retrieved water vapour concentration used (in preference to climatology) to model these contributions in other channels.

In principle, temperature, pressure and the various species profiles can also be retrieved jointly. Joint retrievals are theoretically preferable since each profile can be retrieved from its contributions to *all* other channels or microwindows, not just a subset. However this is computationally more expensive, and the CPU time may be better invested in improving the accuracy of the radiative transfer calculation.

### 5.4 Horizontal Gradients

As mentioned at the beginning, the limb-viewing geometry is intrinsically two-dimensional so that radiances are not only a function of the atmosphere at the profile locations but also the horizontal variations in these parameters, particularly between the tangent point and the satellite.

The current MIPAS retrieval ignores this aspect and regards the atmosphere as having vertical structure only —

a one-dimensional retrieval. This is not unreasonable if only optically thin radiances are used since any linear gradient contributions either side of the tangent point will cancel out. In fact, the error due to a 1K/100 km temperature gradient is included in the microwindow selection so that optically thick regions are avoided and contributions included in the overall systematic error budget. For a near-real-time processor this has the advantage that each limb scan can be processed independently.

The baseline for the HIRDLS retrieval is to perform a two-pass retrieval through an orbit. The first pass is a pure one-dimensional retrieval, but in the second pass, the forward model incorporates gradients determined from the first pass. Considering the ray-path structure of the MIPAS nominal scan (Fig. 2), it may be possible to do this with a single pass stepping backwards in time (right to left in the Figure) since the raypaths for one profile will mostly pass through only later profiles.

The ultimate solution is a full two-dimensional, or 'tomographic' retrieval, which has been suggested for a future version of the MIPAS operational processor. To avoid boundary effects it may also be possible to treat an entire orbit from summer pole to summer pole as a closed circle — adjacent orbits intersect close to this point and if the atmosphere is zonally symmetric the horizontal structure should be very similar in the end segments of each orbit.

Apart from improved accuracy, one further advantage of modelling the horizontal structure is that the retrieved profile can be defined to lie along a true vertical rather than the tangent point locations.

### 5.5 Retrieval Schemes

There are three basic types of retrieval scheme in use, depending on the cost function $\chi^2$ to be minimised (Rodgers, 2000).

Least Squares Fit:

$$\chi^2 = (\mathbf{y}-\mathbf{F}(\mathbf{x}))^T \mathbf{S}_y^{-1} (\mathbf{y}-\mathbf{F}(\mathbf{x})) \tag{11}$$

where $\mathbf{y}$ are the measured spectra, $\mathbf{F}(\mathbf{x})$ are the modelled spectra for state vector $\mathbf{x}$, and $\mathbf{S}_y$ is the measurement covariance matrix. This has the advantage of maximum vertical resolution but tends to be unstable, often leading to vertically 'oscillating' profiles. It also requires good information on every parameter in the state vector.

Tikhonov Regularisation:

$$\begin{aligned}\chi^2 &= (\mathbf{y}-\mathbf{F}(\mathbf{x}))^T \mathbf{S}_y^{-1} (\mathbf{y}-\mathbf{F}(\mathbf{x})) \\ &\quad +\gamma(\mathbf{R}\mathbf{x})^T (\mathbf{R}\mathbf{x})\end{aligned} \tag{12}$$

where $\mathbf{R}$ is typically a first or second derivative operator, and $\gamma$ some tunable parameter (not necessarily a scalar). This constrains profiles to be smoother, so trades some vertical resolution for stability. The parameter $\gamma$ can be difficult to adjust.

Optimal Estimation:

$$\begin{aligned}\chi^2 &= (\mathbf{y}-\mathbf{F}(\mathbf{x}))^T \mathbf{S}_y^{-1} (\mathbf{y}-\mathbf{F}(\mathbf{x})) \\ &\quad +(\mathbf{x}-\mathbf{a})^T \mathbf{S}_a^{-1} (\mathbf{x}-\mathbf{a})\end{aligned} \tag{13}$$

where $\mathbf{a}$ is an *a priori* profile (e.g., climatology) and $\mathbf{S}_a$ its covariance. This constrains the retrieval to fall somewhere between the measurements (as predicted by the least squares fit) and the *a priori* profile, with the weight set by $\mathbf{S}_a$. This biases the retrieval towards the *a priori* so consequently $\mathbf{S}_a$ is often set larger than physically realistic (i.e., the climatological uncertainty) in order to serve as a purely mathematical constraint over most of the profile range.

The current MIPAS operational retrieval is nominally a least squares fit — it has the option of regularisation but this is switched off. However, since the retrieval is an iterative scheme which is not run to convergence, there is some regularising effect from the residual value of the Levenberg-Marquardt parameter. HIRDLS will use optimal estimation.

## 6 Summary

The advantages of infrared limb-sounding are improved vertical resolution and the combination of longer path-lengths and cold background which allows additional species to be measured.

The disadvantages are poor horizontal resolution and increased sensitivity to horizontal structure if not handled properly.

Cloud sensitivity is different to nadir-sounders: while the presence of clouds only affects lower tangent heights rather than the whole profile, the viewing geometry significantly increases the chances of cloud contamination.

Finally, the geometry itself imposes additional complexities in the forward modelling and the $p, T$-pointing retrieval, and requires a higher spectral resolution in the radiative transfer modelling.

## Acknowledgements

Details of HIRDLS operations and processing have been supplied by John Barnett (Oxford University) and Alyn Lambert (NCAR).

## References

Clarmann, T. von and G. Echle (1998). Selection of Optimized Microwindows for Atmospheric Spectroscopy. *App. Optics, 37*, 7661–7660.

Echle, G., T. von Clarmann, A. Dudhia, J.-M. Flaud, B. Funke, N. Glatthor, B. J. Kerridge, M. López-Puertas, F. J. Martín-Torres and G. P. Stiller (2000). Optimized Spectral Microwindows for MIPAS-Envisat Data Analysis. *App. Optics, 39*, 5531–5540.

Dudhia, A., V. L. Jay and C. D. Rodgers (2002a). Microwindow Selection for High-Spectral-Resolution Sounders. *App. Optics, 41*, 3665–3673.

Dudhia, A., P. E. Morris and R. J. Wells (2002b) Fast Monochromatic Radiative Transfer Calculations for Limb Sounding. *J. Quant. Spect. Radiative Transfer, 74*, 745–756.

Edwards, D. P., J. C. Gille, P. L. Bailey and J. J. Barnett (1995). Selection of the Sounding Channels for the High Resolution Dynamics Limb Sounder. *Appl. Optics, 34*, 7006–7018.

ESA (2000). Envisat-MIPAS: An Instrument for Atmospheric Chemistry and Climate Research. *ESA SP-1229*. ESTEC, Noordwijk, The Netherlands.

Gille, J. C., J. J. Barnett, W. G. Mankin, B. R. Johnson, M. Dials, J. G. Whitney, D. Woodard, P. I. Arter, W. P. Rudolph (1994). High Resolution Dynamics Limb Sounder (HIRDLS) for the Earth Observing System. *Proceedings of SPIE, 2266*, 330–339.

Marks, C. J., and C. D. Rodgers (1993). A Retrieval Method for Atmospheric Composition From Limb Emission Measurements. *J. Geophys. Res., 98*, 14939–14953.

Ridolfi, M., B. Carli, M. Carlotti, T. von Clarmann, B. M. Dinelli, A. Dudhia, J-M. Flaud, M. Höpfner, P. E. Morris, P. Raspollini, G. Stiller and R. J. Wells (2000). Optimized Forward Model and Retrieval Scheme for MIPAS Near-Real-Time Data Processing. *App. Optics, 39*, 1323–1340.

Rodgers, C. D. (2000). *Inverse Methods for Atmospheric Sounding: Theory and Practice*. Singapore: World Scientific.

Weinreb, M. P. and A. C. Neuendorffer (1973). Method to Apply Homogeneous-Path Transmittance Models to Inhomogeneous Atmospheres. *J. Atmos. Sci., 30*, 662–666.